New thermoelastic parameters of natural C2/c omphacite

Physics and Chemistry of Minerals

New thermoelastic parameters of natural C2/c omphacite

--Manuscript Draft--

Manuscript Number:	PCMI-D-11-00099R1
Full Title:	New thermoelastic parameters of natural C2/c omphacite
Article Type:	Original paper
Keywords:	omphacite; high-pressure; high-temperature; single-crystal; X-ray diffraction
Corresponding Author:	Francesco Pandolfo, M.D. Universita' degli Studi di Pavia Pavia, PV ITALY
Corresponding Author Secondary Information:	
Corresponding Author's Institution:	Universita' degli Studi di Pavia
Corresponding Author's Secondary Institution:	
First Author:	Francesco Pandolfo, M.D.
First Author Secondary Information:	
Order of Authors:	Francesco Pandolfo, M.D.
	Fabrizio Nestola, Prof.
	Fernando Cámara, Prof.
	Maria Chiara Domeneghetti, Prof.
Order of Authors Secondary Information:	
Abstract:	The compressibility at room temperature and the thermal expansion at room pressure of two disordered crystals (space group C2/c) obtained by annealing a natural omphacite sample (space group P2/n) of composition close to Jdjavascript:insert_text('%E2%82%85')javascript:insert_text('%E2%82%86')Dijavascript:insert_text('%E2%82%84')javascript:insert_text('%E2%82%84') and Jdjavascript:insert_text('%E2%82%85')javascript:insert_text('%E2%82%85')Dijavascript:insert_text('%E2%82%84')javascript:insert_text('%E2%82%85'), respectively, have been studied by single crystal X-ray diffraction. Using a Birch-Murnaghan equation of state truncated at the third-order [BM3-EoS] we have obtained the following coefficients: Vjavascript:insert_text('%E2%82%80')= 421.04(7) Åjavascript:insert_text('%C2%B3'), Kjavascript:%20%20insert_text('%CF%84')javascript:insert_text('%E2%82%80') = 119(2) GPa, K' = 5.7(6). A parameterized form of the BM3 EoS was used to determine the axial moduli of a, b, and c. The anisotropy scheme is Kcjavascript:insert_text('%E2%89%A4')Kajavascript:insert_text('%E2%89%A4')Kb, with an anisotropy ratio 1.05:1.00:1.07. A fitting of the lattice variation as a function of temperature, allowing for linear dependency of the thermal expansion coefficient on the temperature yielded αjavascript:%20%20insert_text('%CE%BD')(1bar,303K) = 2.64(2)*10javascript:insert_text('%C2%AF')javascript:insert_text('%E2%81%B5')Kjavascript:insert_text('%C2%AF')javascript:insert_text('%C2%B9') and an axial thermal expansion anisotropy of αb >> αa > αc. Comparison of our results with available data on compressibility and thermal expansion shows that while a reasonable ideal behaviour can be proposed for the compressibility of clinopyroxenes in the jadeite-diopside binary join [Kjavascript:%20%20insert_text('%CF%84')javascript:insert_text('%E2%82%80') as a function of Jd molar %: Kjavascript:%20%20insert_text('%CF%84')javascript:insert_text('%E2%82%80') = 106(1) GPa + 0.28(2)xJd(mol%)], the available data has not sufficient quality to extract the behaviour of thermal expansion for the same binary join in terms of composition.

New thermoelastic parameters of natural *C*2/*c* omphacite

FRANCESCO PANDOLFO[1,*], FABRIZIO NESTOLA[2], FERNANDO CÁMARA[3], M. CHIARA DOMENEGHETTI[1]

[1]Dipartimento di Scienze della Terra e dell'Ambiente, Università di Pavia, via Ferrata 1, I-27100 Pavia, Italy
[2]Dipartimento di Geoscienze, Università di Padova, via Gradenigo 6, I-35131 Padova, Italy
[3]Dipartimento di Scienze della Terra, Università degli Studi di Torino, via Valperga Caluso 35, I-10125 Torino, Italy
*E-mail: francesco.pandolfo@unipv.it

ABSTRACT

The compressibility at room temperature and the thermal expansion at room pressure of two disordered crystals (space group *C*2/*c*) obtained by annealing a natural omphacite sample (space group *P*2/*n*) of composition close to $Jd_{56}Di_{44}$ and $Jd_{55}Di_{45}$, respectively, have been studied by single crystal X-ray diffraction. Using a Birch-Murnaghan equation of state truncated at the third-order [BM3-EoS] we have obtained the following coefficients: V_0 = 421.04(7) Å^3, K_{T0} = 119(2) GPa, K' = 5.7(6). A parameterized form of the BM3 EoS was used to determine the axial moduli of *a*, *b*, and *c*. The anisotropy scheme is $\beta_c \leq \beta_a \leq \beta_b$, with an anisotropy ratio 1.05:1.00:1.07. A fitting of the lattice variation as a function of temperature, allowing for linear dependency of the thermal expansion coefficient on the temperature yielded $\alpha_{V(1bar,303K)} = 2.64(2)\cdot10^{-5}K^{-1}$ and an axial thermal expansion anisotropy of $\alpha_b >> \alpha_a > \alpha_c$. Comparison of our results with available data on compressibility and thermal expansion shows that while a reasonable ideal behaviour can be proposed for the compressibility of clinopyroxenes in the jadeite-diopside binary join [K_{T0} as a function of Jd molar %: K_{T0} = 106(1) GPa + $0.28(2)\times Jd_{(mol\%)}$], the available data has not sufficient quality to extract the behaviour of thermal expansion for the same binary join in terms of composition.

Key-words: omphacite, high-pressure, high-temperature, single-crystal, X-ray diffraction

INTRODUCTION

Omphacitic clinopyroxenes and pyropic garnet represent the main constituents of mantle-derived eclogite; therefore, their behaviour under extreme conditions of temperature and pressure provides clues to the conditions under which the eclogite formed (e.g. Nestola et al. 2007). In particular omphacite, if crystallized above about 850°C, shows space group *C*2/*c* whereas below such temperature a lower symmetry *P*2/*n* is found (Carpenter 1981). This clinopyroxene has been also found as inclusion in natural diamonds: the assemblage garnet + omphacite in diamond is very important as it immediately provides the eclogitic origin of the diamond itself. In

addition, knowing the thermoelastic properties (e.g. thermal expansion and compressibility) of omphacite would be extremely useful to perform a systematic comparison of the pressure formation for eclogitic diamonds (Nestola et al. 2011).

Despite disordered omphacite represents a crucial high-pressure phase, thermoelastic data are available at present only from few studies. In particular, the compressibility study by McCormick et al. (1989) was performed on vacancy-bearing *C*2/*c* omphacite samples, that by Baghat et al. (1992) was performed on a $Jd_{66}Di_{34}$ sample and the most recent work was carried out by Nishihara et al. (2003) on a $Jd_{37}Di_{63}$ sample. Two further studies have been performed on ordered *P*2/*n* omphacite by Pavese et al. (2001) by means of powder diffraction and by (Pandolfo et al. 2011) by single crystal X-ray diffraction. Concerning the thermal expansion data to our knowledge there is only one study on a *P*2/*n* sample (Pavese et al. 2000).

In this work we aim to determine experimentally with high accuracy and precision the compressibility and the thermal expansion of a disordered omphacite (space group *C*2/*c*) by single-crystal X-ray diffraction (SCXRD) using a diamond-anvil cell for high pressure conditions and a microfurnace for high-temperature conditions. Our results could be thus directly used to obtain reliable geo-barometric data.

EXPERIMENTAL METHODS

Sample characterization

Two twin and inclusion-free single crystals of *P*2/*n* omphacite from sample 74AM33 with an appropriate size were selected for single crystal X-ray diffraction (SCXRD) experiments and labeled as N2 and N3. Sample 74AM33 is from Münchberg Mass (Bavaria) eclogitic rock and it was previously studied by Boffa Ballaran et al. (1998). Electron microprobe analysis (EMPA) of 74AM33 sample was carried out at the Dipartimento di Geoscienze, University of Padova, using a CAMECA CAMEBAX electron microprobe in wavelength-dispersive (WDS) mode, operating in wavelength dispersive mode with a fine-focused beam (~1 mm diameter), an acceleration voltage of 20 kV and a beam current of 10 nA, with 10 s counting times for both peak and total background. X-ray counts were converted to oxide wt.% using the PAP correction program supplied by CAMECA (Pochou and Pichoir, 1991). Standards, spectral lines, and analytical crystals used were: albite (Na-Ka, TAP), wollastonite (Si, Ca-Ka, TAP), olivine (Mg-Ka, TAP), Al_2O_3 (Al-Ka, TAP), $MnTiO_3$ (Mn-Ka, LiF; Ti- Ka, PET), Cr_2O_3 (Cr-Ka, LiF), Fe_2O_3 (Fe-Ka, LiF). The chemical analysis of the sample 74AM33, crystal N3, is reported in Table 1. It was no possible to recover crystal N2 after the high-temperature experiment. However, the two crystals N2 and N3 can be assumed having practically the same chemical composition as

shown by the differences in their unit-cell volumes (Table 2), which exhibit maximum discrepancy values lower than 0.2%.

Single crystal X-ray diffraction at ambient conditions and disordering experiment

The SCXRD analyses at ambient conditions and the annealing experiment to obtain *C*2/*c* omphacite samples were carried out at the Dipartimento di Scienze della Terra e dell'Ambiente, University of Pavia. Preliminary analysis, performed on crystals N2 and N3, using a Philips PW1100 four-circle automated diffractometer with graphite monochromator and Mo*K*α radiation, showed sharp diffraction profiles and yielded high precision unit-cell parameters. These data are in agreement with the previous published cell-parameters by Boffa Ballaran et al. (1998). The intensity data of two crystals were collected on a three-circle Bruker AXS SMART APEX diffractometer, equipped with a CCD detector (graphite-monocrhromatized MoKα radiation λ=0.71073 Å, 50 kV, 30 mA) and a MonoCap collimator. The Bruker SMART v.5.625 software package was used for collection images. A total of 3360 frames (frame resolution 512x512 pixels) were collected with four different goniometer settings using the ω-scan mode (scan width: 0.2 °ω; exposure time: 10 s; detector sample distance 4.02 cm). Completeness of the measured data was achieved up to 78° 2θ. The Bruker SAINT+ v.6.45 software was used for data reduction, including intensity integration and background and Lorentz-Polarization corrections. The semi-empirical absorption correction of Blessing (1995), based on the determination of transmission factors for equivalent reflections, was applied using the program SADABS (Sheldrick 1996) and the monoclinic Laue group 2/*m*. The intensity data were refined in the *P*2/*n* space group starting from the atomic coordinates by Pavese et al. (2000). Structural refinements were carried out using program SHELX-97 (Sheldrick 1997). The atomic scattering curves were taken from the *International Tables for X-ray Crystallography* (Wilson 1995). Neutral vs. ionized scattering factors were refined for all sites that are not involved in chemical substitutions (O and Si) (Hawthorne et al. 1995). When the refinement reached convergence, full-matrix least-squares were carried out using the data from the electron microprobe analysis (with 1σ error) as chemical constraints to obtain the site partitioning using the same procedure already described in Pandolfo et al. (2011). Observed degrees of order calculated as Carpenter et al. (1990) for these two natural crystals are reported in Table 2.

An annealing experiments on the two crystals was carried out using a vertical temperature-controlled furnace [±3 °C, chromel-alumel thermocouple] to obtain completely disordered (*C*2/*c*) omphacite crystals. The crystals were loaded in a platinum crucible and were sealed into a silica glass tube, after alternately washing with Ar flux and vacuuming. This isothermal heating experiment was performed at 1000 °C for 300 hrs and quenched by dropping the tube into cold water.

The crystals were then mounted again on the Bruker AXS SMART APEX diffractometer, using the same conditions as described above. Due to the verified absence of reflections $h+k = 2n+1$, the intensity data were then refined as described before, in the $C2/c$ space group starting from the atomic coordinates previously reported by McCormick et al. (1989). Lattice parameters for the crystals before and after their annealing are reported in Table 2.

When the refinement reached convergence, full-matrix least-squares were carried out using the data from the electron microprobe analysis (with 1σ error) as chemical constraints to obtain the site partitioning. The following restraints were introduced into the refinement: (1) all structural sites were considered fully occupied; (2) Al^{3+} was distributed between T and M1; (3) Cr, Mn and Ti were considered fully ordered at M1; (4) Mg and Fe^{2+} were present in both M1 and M2 sites; (5) charge balance was ensured by the equation $X_{Na}^{M2} = X_{Al3+} + X_{Al}^{M1} + 2X_{Ti} + X_{Cr}$. The values of the conventional agreement factor $R1$ as well as other details from the chemical constrained structure refinements are reported in Table 2 together with the mean atomic numbers (m.a.n.) at the M1 and M2 sites. The crystal chemical formula obtained with this procedure is $(Ca_{0.464}Na_{0.502}Mg_{0.033})(Fe_{0.061}Mg_{0.414}Al_{0.519}Cr_{0.002}Ti_{0.003})(Al_{0.025}Si_{1.975})O_6$ for sample N2 and is $(Ca_{0.482}Na_{0.488}Fe_{0.004}Mg_{0.026})(Fe_{0.064}Mg_{0.420}Al_{0.511}Cr_{0.002}Ti_{0.003})(Al_{0.031}Si_{1.969})O_6$ for sample N3. The compositions of our samples expressed in end-member mol % are: $Jd_{49}Di_{38}Hd_6CaTs_3En_3Ko_1$ for N2 and $Jd_{48}Di_{40}Hd_5CaTs_3En_2Fs_1Ko_1$ for N3. In order to compare our data with jadeite and diopside end-members hereafter we will refer to a composition $Jd_{56}Di_{44}$ for N2 and $Jd_{55}Di_{45}$ for N3 sample, obtained renormalizing their composition to 100% of Jd – Di. The full structural data are also been deposited as cifs[1].

Single-crystal high-pressure X-ray diffraction

The high-pressure SCXRD experiments were carried out at the Dipartimento di Geoscienze, University di Padova. Crystal N3 was loaded in an ETH-type DAC (Miletich et al. 2000) using a steel gasket (T301), pre-indented to a thickness of 110 μm and with a 250 μm diameter hole. A single crystal of quartz was used as internal diffraction pressure standard (Angel et al. 1997) and a 16:3:1 mixture of methanol:ethanol:water was used as hydrostatic pressure medium, which remains hydrostatic up to about 9.5-10 GPa (Angel et al. 2007). Unit-cell parameters were determined at 13 different pressures up to about 7.5 GPa using a STOE STADI-IV four-circle diffractometer (operating at 50 kV and 40 mA) automated by SINGLE software (Angel and Finger 2011). The unit-cell parameters were measured centering about 20 reflections for each high-pressure experiment. Full details of the instrument and the peak-centering algorithms are provided by Angel et al. (2000). During the centering procedure the effects of crystal offsets and diffractometer aberrations were eliminated from refined

peak positions by the eight-position centering method of King and Finger (1979). Unit-cell parameters, obtained by vector least-squares (Ralph and Finger 1982) are reported for each pressure step in Table 3.

Single-crystal high-temperature X-ray diffraction

High-temperature experiment was carried out at the Dipartimento di Scienze della Terra e dell'Ambiente, University of Pavia using a Philips PW1100 four-circle automated diffractometer working with Mo*K*α radiation at 30 mA/55 kV and using a 0.5 mm collimator, and operated with FEBO software (a local developed control software) equipped with a microfurnace for in-situ high-temperature experiments consisting of a H-shaped Pt-Rh resistance and a Pt:Pt-Rh thermocouple inside a steel cylindrical cage 1 inch wide closed with a Kapton film. The device allows the collection of diffraction data up to θmax=29°.

Crystal N2 was loaded in a 0.3 mm inner diameter quartz vial 26 mm long closed at the top by using oxy-methane flame. To avoid any mechanical stress the crystal was kept in position within the vial using quartz wool. A graphite powder was loaded in the vial close to the crystal in order to act as a buffer to avoid Fe oxidation during the annealing.

A temperature calibration of the microfurnace was undertaken by observing the melting of eight selected pure salts and measuring the thermal expansion of a spherical crystal of quartz across the α-β phase transition mounted as described before. Linear fitting performed on the observed melting points and on the observed transition temperature for the α-β quartz phase transition with the recorded temperature at the controller display yielded the following equation:

$$(1)\ T = -8.818(4.684) + 1.154(10) \times T\text{display}$$

Stability of temperature of the furnace while changing goniometer position was within a few units of K. For more details on microfurnace calibration see Cámara et al. (2011).

Preliminary cell centering was performed using 24 intense reflections over the 2θ interval 15–30 using horizontal and vertical slits. Accurate and precise lattice constants were then determined using the Philips LAT procedure based on the least-squares refinement of the UB-matrix on the basis of the 60 most intense reflections measured in a data collection mode where the position of each diffraction spot were measured in positive and negative ω-2θ by first centering the spot, using the vertical and horizontal slits, then performing a selected scan in ω-2θ and calculating the observed maxima. The same set of reflections was used for each temperature measurement. Lattice parameters were collected at intervals of 50K in the T range 303-1073K for the increasing and decreasing temperature trends. We conducted the whole experiment up to the 1073K and down to room temperature in about 110 hours. In particular high-T data > 873K were collected in only 25 hours to hamper the ordering kinetics. For each temperature datum we also collected intensities for selected reflections with $h + k = 2n+1$ ($\bar{1}$

0 1, 0 5 0) and $h + k = 2n$ ($\bar{2}$ 0 2, 0 6 0). For each reflection we collected intensities five times in order to obtain a statistical representative value. The absence of intensities > 3σ for superstructure reflections (i.e. $h + k = 2n+1$) in both the increasing and decreasing trends ensured that the crystal kept disorder for the whole experiment. Unit-cell parameters for each step, increasing and decreasing temperature, are reported in Table 4.

RESULTS

Evolution of the unit-cell parameters with pressure and P – V equation of state

The evolutions of the unit-cell parameters and unit-cell volume with pressure are shown in Figure 1 and 2. A continuous decrease of *a*, *b*, *c*, β angle and volume, *V*, is observed as a function of pressure with no evidence of a phase transition up to the maximum pressure reached. The *a*, *b*, *c* lattice parameters decrease by about 1.7, 2.0 and 1.8% up to 6.9 GPa, respectively, β by 0.6% and the unit-cell volume decreases by about 5.0%.

In order to define the best equation of state that adequately describes the pressure-volume trend for the sample here studied an F_E-f_E plot was constructed following Angel (2000) and is shown in Figure 3. The plot shows that the data lie on a positively inclined straight line indicating that a Birch-Murnaghan equation of state truncated at the third-order [BM3-EoS, Birch (1947)] must be used to fit the experimental pressure-volume data. Thus, using EoS-FIT 5.2 software (Angel 2002) it was possible to refine simultaneously to a BM3 the volume, V_0, the bulk modulus K_{T0}, and its first pressure derivative K' obtaining the following coefficients: V_0 = 421.04(7) Å^3, K_{T0} = 119(2) GPa, K' = 5.7(6). The quality of the experimental data is demonstrated by the small differences between the EoS coefficients obtained by the refinement and by the F_E-f_E plot of Figure 3 [K_{T0} = 117(1) GPa, K' = 6.1(3)]; the intercept corresponds to the bulk modulus whereas the slope of the straight line provides the first pressure derivative as in Angel (2000).

A parameterized form of the BM3 EoS was used to determine the axial moduli of *a*, *b*, and *c* again using EoS-FIT5.2. All the equation-of-state coefficients together with the relative axial compressibilities are reported in Table 5. The anisotropy scheme is $\beta_c \leq \beta_a \leq \beta_b$, with an anisotropy ratio 1.05:1.00:1.07. It is remarkable that, as in other clinopyroxenes, the stiffest direction resulted to be *a*senβ (e.g Nestola et al. 2004).

Evolution of the unit-cell parameters with temperature and thermal expansion equations

The evolution of the unit-cell parameters and cell volume with temperature is reported in Figure 4 and 5. A continuous increasing of the unit-cell parameters and volume is observed as a function of temperature with no evidence of a phase transition up to the maximum temperature reached. Data collected both increasing and decreasing temperature overlap within experimental error. Therefore for the following estimation of thermal

expansion coefficient we used only the data on increasing temperature. The *a*, *b*, *c* lattice parameters increase by about 0.7, 1.1 and 0.6 % up to 1073K, respectively, β by 0.1 % and the unit-cell volume increases by about 2.3%. Thermal expansion is defined as $\alpha_{(V,T)} = 1/V\left(\partial V/\partial T\right)_P$.In order to calculate the volume thermal expansion coefficient we have used different equations to our $T - V$ experimental data. To a first approximation, the coefficient of volume thermal expansion is *T*-independent, and so the variation of the unit-cell volume of our sample with *T* can be fitted by least-squares to the equation by Gottshalk (1997):

$$(2)\ V(T) = V_0(P_r, T_r)e^{\alpha_0(T-T_r)}$$

where $V_o(P_r,T_r)$ is the volume of the phase at reference pressure and temperature, α_o is the volume thermal expansion coefficient and T_r is the reference temperature. The derived coefficients of volume and axial thermal expansion data are: $\alpha_{V(1bar,303K)}$ 3.03(3)·10^{-5}K^{-1}, $\alpha_{a(1bar,303K)}$ = 0.90(1)·10^{-5}K^{-1}, $\alpha_{b(1bar,303K)}$ = 1.48(1)·10^{-5}K^{-1} and $\alpha_{c(1bar,303K)}$ = 0.72(1)·10^{-5}K^{-1}, with a temperature anisotropy of $\alpha_b >> \alpha_a > \alpha_c$. Nevertheless, it is well known that α varies with *T* in a non-linear way analogous to that of the heat capacity, i.e. asymptoting at very high *T*. This can be seen by calculating the components of the thermal expansion tensor at each experimental point and plotting their variation with temperature (see by instance Redhammer et al. 2010 for one example on one synthetic clinopyroxene). This non-linearity can be fitted with a physical model involving the vibrational density of states (Anderson et al. 1992) or a quasi-harmonic Einstein model as described by Knight (1996). These procedures require high-quality data collected well below room-*T*, which are not available in this study.

Empirical fits can be used instead for the purpose of accounting for the dependence of α on *T* when fitting *T* - *V* experimental data over a specific temperature range. A polynomial equation expressing the thermal expansion coefficient α as a function of temperature may be used, as that one proposed by Fei (1995):

$$(3)\ V(T) = V_{T_r}\exp\left[\int_{T_r}^{T}\alpha(T)dT\right]$$

where the value of the thermal expansion coefficient is $\alpha_{(V,T)} = a_0 + a_1T + a_2T^{-2}$. Applying this equation truncated at the first order of the polynomial to our omphacite *T* - *V* data we obtain $\alpha_{V(1bar,303K)}$ 2.64(3)·10^{-5}K^{-1}.

Another widely used equation, which expresses the volume as a function of temperature is the second-order polynomial of Berman (1988):

$$(4)\ V(T) = V_{0(P_r,T_r)}\left[1 + a_1(T - T_r) + a_2(T - T_r)^2\right]$$

A first differentiation this equation gives $\alpha_{(V,T)} = a_1 + 2a_2(T - T_r)$. Applying it to the omphacite volume data we obtain $\alpha_{V(1bar,303K)}$ = 2.64(2)·10^{-5}K^{-1}. At room temperature conditions, i.e. $T = T_r$, the value of α is equal to a_1. The truncation to the first order of the polynomial in the approximation of Fei (1995) yields very similar results (Table 6). Nevertheless, the polynomial model can only achieve a correct prediction with the addition of a further term allowing for saturation of α at high-T [for example it could be possible in Fei (1995)] but fitting this term produces a small a_2 coefficient with an observed standard deviation comparable to the value itself, and therefore we opted for the first order truncation. To avoid difficulties fitting experimental data a single-parameter model can be adjusted to account for non-linear behaviour and high-T saturation of α as was proposed by Holland and Powell (1998), with:

$$(5)\ V(T) = V_{0(\mathrm{Pr},Tr)}\left[1 + a_0(T - T_r) + 20a_0(\sqrt{T} - \sqrt{T_r})\right]$$

in which the thermal expansion at any given temperature can be obtained from $\alpha_{(V,T)} = a_0(1 - 10/\sqrt{T})$. The derived coefficients of volume and axial thermal expansion data using such equation applied to our omphacite data are: $\alpha_{V(1bar,303K)}$ = 2.16·10^{-5}K^{-1}, $\alpha_{a(1bar,303K)}$ = 0.64·10^{-5}K^{-1}, $\alpha_{b(1bar,303K)}$ = 1.05(2)·10^{-5}K^{-1}and $\alpha_{c(1bar,303K)}$ = 0.51·10^{-5}K^{-1} showing a room temperature anisotropy of $\alpha_b >> \alpha_a > \alpha_c$. The derived coefficients for axial thermal expansion data calculated at high temperature (1073K) are $\alpha_{a(1bar,1073K)}$ = 1.04·10^{-5}K^{-1}, $\alpha_{b(1bar,1073K)}$ = 1.71(2)·10^{-5}K^{-1}and $\alpha_{c(1bar,1073K)}$ = 0.83·10^{-5}K^{-1} and thus maintaining the same anisotropy scheme observed at room-T conditions.

All the volume thermal expansion data obtained using the above equations for our studied disordered omphacite crystal are reported in Table 6. In Figure 5 the relative V/V_0 variation is plotted versus the temperature. In this Figure, the experimental $T - V$ data have been fitted with the different equations: it is quite evident that the Gottshalk (1997) linear trend (in red) does not represent satisfactorily our data, whereas the equation by Holland and Powell (1998) (in blue) does not show a good fitting for temperatures between about 500 and 800K. Finally, the two equations by Berman (1988) and Fei (1995) perfectly fit our data and are totally overlapped (we represented therefore the two curves with the same black color) in the Figure 5, in agreement with the volume thermal expansion coefficients, which are identical for these two equations (see Table 6). In general, based on the different experimental data fitting we consider the value of $\alpha_{V(1bar,303K)}$ = 2.64(2)·10^{-5}K^{-1} as the most accurate for disordered omphacite.

DISCUSSIONS AND CONCLUSIONS

The data obtained for our omphacite samples gave us a volume thermal expansion $\alpha_{V(1bar,303K)} = 2.64(2)\cdot10^{-5}K^{-1}$ and a bulk modulus K_{T0} = 119(2) GPa with a K′ = 5.7(6).

Thermal expansion data on the pure end-members jadeite (data from Tribaudino et al. 2008) and diopside (data from Finger 1976) were recalculated using Berman (1988) equation, providing $\alpha_{V(1bar,303K)} = 2.1(1)\cdot10^{-5}K^{-1}$ and $2.8(2)\cdot10^{-5}K^{-1}$, respectively (Table 6). These data and that relative to our sample N3 are plotted versus the Jd molar % in Figure 6. We observe that the α_V does not show any variation from diopside to our composition within 1σ, whereas it decreases by about 19% from our composition to pure jadeite. It is evident that the samples along the join do not lie on a linear trend. The large sigma values that we obtained for jadeite and diopside are due to the scarce number of experimental $T - V$ data. In our opinion it would be convenient to reinvestigate the thermal expansion behaviour of diopside and jadeite and other compositions along the join, using the same experimental procedures followed in our work. With this approach, we could be able to obtain a reliable comparison and provide a final equation able to constrain the thermal expansion coefficient of a sample along the Jd-Di join.

Concerning the bulk modulus data, we have compared the values relative to sample $Jd_{55}Di_{45}$ (*C*2/*c* sample N3, this work, and *P*2/*n* sample N4 by Pandolfo et al. 2011) with those of jadeite (Nestola et al. 2006), diopside (Gavrilenko et al. 2010) and of two vacancy bearing omphacites by McCormick et al. (1989) (see Figure 7). We have not used for comparison the data by Nishihara et al. (2003) as this work was performed at variable HP/HT conditions using the synchrotron radiation inside a multi-anvil press. This procedure is not recommended to provide accurate data of bulk modulus (Angel et al. 2009). The bulk modulus value provided by Baghat et al. (1992), obtained by Brillouin spectroscopy at room pressure conditions, was not considered in this comparison as in such study the first pressure derivative could not be determined. As matter of fact, it is obvious that the bulk modulus values obtained refining simultaneously the K_{T0} and its first pressure derivative (see our study, Gavrilenko et al. 2010, Nestola et al. 2006) and those obtained without indication of the first pressure derivative cannot be easily compared. In Figure 7 it is evident that bulk modulus data of jadeite (Nestola et al. 2006), our $Jd_{55}Di_{45}$ sample, and diopside (Gavrilenko et al. 2010) lie on a linear trend. It is also worth to note that: i) the ordered *P*2/*n* and disordered *C*2/*c* omphacite overlap within the experimental errors; ii) the vacancy poor sample by McCormick et al. (1989) lies out of the above reported linear trend further than the vacancy rich one. The cause of such discrepancy observed in McCormick et al. (1989) data cannot be explained in terms of structural vacancies but is probably due to: a) limited value of high pressure reached during the experiment (e.g. 6 GPa); b) a limited number of $P - V$ experimental data (i.e. 6 data points); c) a calibration of experimental pressure done

using the ruby fluorescence instead of the quartz EoS (which was used in the other high-pressure experiments); d) the impossibility to refine the first pressure derivative.

Using the data by Gavrilenko et al. (2010), Pandolfo et al. (2012) and Nestola et al. (2006) plotted in Figure 7, we obtained the following weighted linear equation, which expresses the evolution of K_{T0} as a function of Jd molar %:

$$(6)\ K_{T0} = 106(1)\ \text{GPa} + 0.28(2) \times \text{Jd}_{(\text{mol}\%)}$$

Such equation clearly indicates that for *C*2/*c* disordered omphacite the bulk modulus increases linearly with the Jd molar % from 106 to 134 GPa (accounting for a maximum increase by about 21%).

Concerning the first pressure derivative, $K`$, as found in previous clinopyroxenes investigated using the same experimental techniques used in this work, it seems to be closely related to the change in cation radius at M2 site. Analysing previous data on jadeite-aegirine (Nestola et al. 2006), jadeite-hedenbergite (Nestola et al. 2008) and kosmochlor-diopside (Boffa Ballaran et al. 2009) solid solutions it is evident that when a single cation is present over the entire join (i.e. jadeite-aegirine) the first pressure derivative remains constant, whereas when at M2 site an Na-Ca substitution occurs the first pressure derivative changes as a function of such substitution. This results in an increase in $K`$ value with increasing the cation radius at M2 site. Our data show that this observation can be applied also to the jadeite-diopside join.

Our results thus indicate that the behaviour of bulk modulus in the jadeite – diopside solid solution is ideal, and that the convergent order in omphacite does not influence the bulk modulus value. Therefore, equation (6) is what we consider the best fit using the most recent, accurate and comparable data today available in literature and can be readily used as a compressibility predicting model for any composition along the join.

ACKNOWLEDGEMENTS

Roberto Gastoni CNR-Pavia is thanked for sample preparation for EMPA analyses and R. Carampin of CNR-Padova is thanked for help with the WDS electron microprobe facilities. This work was funded by the Italian Ministry of University and Research (MIUR) and by F.A.R. of the University of Pavia. The paper benefited from the critical reviews of two anonymous reviewers and Editor Milan Rieder.

REFERENCES

Anderson OL, Isaak D, Oda HT (1992) High temperature elastic constant data on minerals relevant to geophysics. Rev in Geophysis 30: 57-92

Angel RJ (2000) Equations of State. In R.M. Hazen and R.T. Downs, Eds., High-Temperature and High-Pressure Crystal Chemistry. Rev Mineral Geochem vol 41. pp. 35-39

Angel RJ (2002) EOSFIT V5.2 program. Crystallography Laboratory. Virginia Tech, U.S.A.

Angel RJ and Finger LW (2011) SINGLE: a program to control single-crystal diffractometers. J Appl Cryst 44: 247-251

Angel RJ, Jackson JM, and Speziale S (2009) Elasticity measurements on minerals: a review. Eur J Mineral 21:525-550

Angel RJ, Allan DR, Miletich R, and Finger LW (1997) The use of quartz as an internal pressure standard in high pressure crystallography. J Appl Cryst 30:461-466.

Angel RJ, Bujak M, Zhao J, Gatta D, Jacobsen SD (2007) Effective hydrostatic limits of pressure media for high-pressure crystallographic studies. J Appl Cryst 40:26-32

Bhagat SS, Bass JD, Smith JR (1992) Single-Crystal elastic proprieties of omphatice *C*2/*c* by brillouin scattering spectroscopy. J Geophys Research 97:6843-6848

Berman RG (1988) Internally-consistent thermodynamic data for minerals in the system Na_2O-K_2O-CaO-MgO-FeO-Fe_2O_3-Al_2O_3- SiO_2-TiO_2-H_2O-CO_2. J Petrol 29:445-522

Birch F (1947) Finite elastic strain of cubic crystals. Physical Review 71:809-824

Boffa Ballaran T, Carpenter MA, Domeneghetti MC, Tazzoli V (1998) Structural mechanisms of solid solution and cation ordering in augite-jadeite pyroxenes: I. A macroscopic perspective. Am Mineral 83:419-433

Boffa Ballaran, T., Nestola, F., Tribaudino, M. and Ohashi, H. (2009) Bulk modulus variation along the diopside–kosmochlor solid solution. European Journal of Mineralogy 21:591-597

Cámara F, Gatta D, Meven M, Pasqual D (2011) Thermal expansion and high temperature structure evolution of zoisite by single crystal X-ray and neutron diffraction. Phys Chem Minerals (DOI: 10.1007/s00269-011-0457-9)

Carpenter MA (1981) Time–temperature transformation (TTT) analysis of cation disordering in omphacite. Contrib Petrol Mineral 8:433-440

Carpenter MA, Domeneghetti MC, Tazzoli T (1990) Application of Landau theory to cation ordering in omphacite I: Equilibrium behavior. Eur J Mineral 2:7-18

Fei Y (1995) Thermal expansion, in: Ahrens JA (ed), AGU Reference Shelf 2:29-44.

Gavrilenko P, Boffa Ballaran T,Kepler H (2010) The effect of Al and water on the compressibility of diopside. Am Mineral 95:608-616.

Gottshalk M (1997) Internally consistent thermodynamic data forrock-forming minerals in the system SiO_2-TiO_2-Al_2O_3-Fe_2O_3-CaO-MgO-FeO-K_2O-Na_2O-H_2O-CO_2. Eur J Mineral 9:175-223

Hawthorne FC, Ungaretti L, Oberti R (1995) Site populations in minerals: terminology and presentation of results of crystal-structure refinement. Canadian Mineral 33:907-911

Holland TJB, Powell R (1998) An internally consistentthermodynamic data set for phases of petrological interest. J Metamorph. Geology 16:309-343

King HE, Finger LW (1979) Diffracted beam crystal centering and its application to high-pressure crystallography. J Appl Cryst 12:374-378

Knight KS (1996) A neutron powder diffraction determination of the thermal expansion tensor of crocoite ($PbCrO_4$) between 60 K and 290 K. Mineral Mag 60:963-972

McCormick, TC, Hazen RM, Angel RJ (1989) Compressibility of omphacite to 60 kbar: Role of vacancies. Am Mineral 74:1287-1292

Miletich R, Allan DR, and Kuhs WF (2000) High-pressure single-crystal techniques. In R.M. Hazen and R.T. Downs, Eds., High-Temperature and High-Pressure Crystal Chemistry. Rev Min and Geochem vol. 41 pp. 445-519

Nestola F., Tribaudino M., Boffa Ballaran T. (2004) High pressure behavior transformation and crystal structure of synthetic iron-free pigeonite. Am. Mineral 89:189-196

Nestola, F., Boffa Ballaran, T., Liebske, C., Bruno, M., Tribaudino, M. (2006) High-pressure behaviour along the jadeite $NaAlSi_2O_6$–aegirine $NaFeSi_2O_6$ solid solution up to 10 GPa. Physics and Chemistry of Minerals 33:417-425

Nestola F, Longo M, McCammon C (2007) Crystal-structure refinement of Na-bearing clinopyroxenes from mantle-derived eclogite xenoliths. Am Mineral 92:1242-1245

Nestola F., Boffa Ballaran, T., Liebske, C., Thompson, R. and Downs, R.T. (2008) The effect of the hedenbergitic substitution on the compressibility of jadeite. Am Mineral 93:1005-1013

Nestola F, Nimis P, Ziberna L, Longo M, Marzoli A, Harris JW, Manghnani MH, Fedortchouk Y (2011) First crystal-structure determination of olivine in diamond: Composition and implications for provenance in the Earth's mantle. Earth and Planetary Science Letters 305:249-255

Nishihara Y, Takahashi E, Matsukage K, Kikegawa T (2003) Thermal equation of state of omphacite. Am Mineral 88:80-86

Pavese A, Bocchio R, Ivaldi G (2000) In situ high temperature single crystal X-ray diffraction study of a natural omphacite. Mineral Mag 64:983-993

Pandolfo F, Nestola F, Cámara F, Domeneghetti MC (2012) High-pressure behavior of *P*2/*n* omphacite. Am Mineral (DOI: 10.2138\am.2012.3928)

Pouchou JL, Pichoir F (1991) Quantitative analysis of homogeneous or stratified microvolumes applying the model "PAP." In Electron probe quantitation, edited by Heinrich K. F. J. and Newbury D. E. New York: Plenum Press 31-75

Ralph RL, Finger LW (1982) A computer program for refinement of crystal orientation matrix and lattice constraints from diffractometer data with lattice symmetry constraints. J Appl Cryst 15:537-539

Redhammer GJ , Cámara F, Alvaro M, Nestola F, Tippelt G, Prinz S, Simmons J, Roth G, Amthauer G (2010) Thermal expansion and high-temperature $P2_1/c$-$C2/c$ phase transition in clinopyroxene-type $LiFeGe_2O_6$ and comparison to $NaFe(Si,Ge)_2O_6$. Phys Chem Min 37: 685-704.

Sheldrick GM (1996) SADABS, A Program for Absorption Correction with the Siemens SMART System; University of Gottingen: Gottingen, Germany

Sheldrick GM (1997) SHELX, programs for Crystal Structure Analysis (Release 97-2). Institüt für Anorganische Chemie der Universität, Tammanstrasse 4, D-3400 Göttingen, Germany

Wilson AJC (1995) International Tables for Crystallography. Volume C. Kluwer Academic Publishers, Dordrecht.

Table and Figure captions

Table 1. Chemical composition for the sample 74AM33 studied in this work. Standard deviations of the average of 6 analyses points are reported between parentheses.

Table 2. Unit-cell parameters and structure refinement details for the crystals studied in this work before and after their annealing

Table 3. Unit-cell parameters at different pressure values for crystal N3 studied in this work

Table 4. Unit-cell parameters at different temperature values for crystal N2 studied in this work

Table 5. Equation of state coefficients obtained for the disordered crystal studied using a third order Birch-Murnagnan equation (BM3). Values for Jd (nestola et al. 2006) and Di (Gavr4ilenko et al. 2010) and a BM3 are also reported for comparison.

Table 6. Calculated thermal expansion coefficients for our sample and those obtained fitting previous data on jadeite (Tribaudino et al. 2008) and diopside (Finger 1978).

Figure 1. Relative compression for the unit-cell parameters of $Jd_{56}Di_{44}$ studied in this work.

Figure 2. Unit-cell volume evolution as a function of pressure for the sample investigated in this work. The error bars are smaller than symbols used. The solid curve represents the BM3 equation of state.

Figure 3. $F_E - f_E$ plot for of $Jd_{56}Di_{44}$ here investigated. The solid line is the weighted linear regression.

Figure 4. Relative expansion for the unit-cell parameters of $Jd_{56}Di_{44}$ studied in this work.

Figure 5. Relative volume expansion for $Jd_{56}Di_{44}$ studied in this work. The red line represents the linear fitting relative to the equation (2); the blue curve represents the equation (5) whereas the black curve is relative to equations (3) and (4) which are totally overlapped.

Figure 6. Variation of the volume thermal expansion α_V calculated with eqn. (4) with Jd mol % composition for the available composition of *C*2/*c* pyroxenes along the Jd – Di solid solution.

Figure 7. Variation of the bulk modulus K_{T0} with Jd mol % composition along the Jd – Di solid solution. The line is the plot of eqn. 6.

Table 1.

% oxides		*a.p.f.u.*	
SiO_2	56.5(2)	Si	1.971(8)
TiO_2	0.11(3)	Al^{IV}	0.029(8)
Al_2O_3	13.2(1)	Al^{VI}	0.513(6)
Cr_2O_3	0.08(3)	Fe^{2+}	0.066(8)
FeO	2.3(3)	Mg	0.447(3)
MnO	0.01(1)	Mn	0.0003(4)
MgO	8.60(8)	Ti	0.0030(7)
CaO	12.9(1)	Cr	0.0023(9)
Na_2O	7.1(2)	Ca	0.483(5)
K_2O	0.004(6)	Na	0.48(1)
total	100.8(3)	K	0.0002(3)
		total	3.993(9)

Mn and K were analyzed but the contents found were < 0.01 wt. % and within the standard deviation

Table 2.

	N3		N2	
	before annealing	after annealing	before annealing	after annealing
space group	*P*2/*n*	*C*2/*c*	*P*2/*n*	*C*2/*c*
a (Å)	9.5640(3)	9.5720(5)	9.5556(4)	9.5642(3)
b (Å)	8.7581(3)	8.7482(4)	8.7508(3)	8.7406(3)
c (Å)	5.2539(2)	5.2428(3)	5.2529(2)	5.2493(2)
β (°)	106.942(1)	106.816(1)	106.990(1)	106.856(1)
V (Å^3)	420.98(2)	420.25(4)	420.07(3)	419.97(2)
R_{int} (%)	1.63	1.58	2.1	1.72
R_1 (%)	2.05	2.19	2.12	1.75
wR2	0.056	0.051	0.058	0.0443
n. of *I*/s > 4	1987	1082	2132	1091
n° relf. tot.	2195	1099	2199	1098
ref. param.	110	60	110	60
GooF	1.055	1.23	1.125	1.183
Q_{M1}	0.8869	-	0.8828	-
Q_{M2}	0.5028	-	0.5063	-
m.a.n. M1	13.30(9)	13.31(8)	13.18(9)	13.23(7)
m.a.n. M11	13.80(9)	-	13.71(9)	-
m.a.n. M2	13.48(10)	15.55(14)	13.10(9)	15.15(11)
m.a.n. M21	17.45(9)	-	17.27(9)	-

m.a.n. is the mean atomic number (in electrons per formula unit)

Table 3.

P (GPa)	a (Å)	b (Å)	c (Å)	β (Å)	V (Å^3)
0.00010(1)	9.5741(7)	8.7489(5)	5.252(1)	106.83(1)	421.1(1)
0.545(9)	9.5590(9)	8.734(1)	5.2430(7)	106.78(1)	419.07(8)
1.036(6)	9.5448(6)	8.7197(5)	5.238(1)	106.72(1)	417.5(1)
1.505(6)	9.5331(7)	8.7080(5)	5.231(1)	106.66(1)	416.0(1)
1.64(1)	9.531(1)	8.7042(9)	5.2269(7)	106.66(1)	415.44(9)
2.25(1)	9.5129(9)	8.6890(7)	5.2200(2)	106.62(2)	413.4(2)
2.675(7)	9.5054(9)	8.6790(9)	5.2132(6)	106.55(1)	412.25(7)
3.44(1)	9.4851(7)	8.6602(6)	5.2027(8)	106.47(1)	409.84(8)
4.04(1)	9.4753(9)	8.642(1)	5.1953(5)	106.41(1)	408.11(7)
4.43(1)	9.4636(8)	8.6379(7)	5.1902(6)	106.390(9)	407.04(6)
5.13(1)	9.4516(7)	8.6191(7)	5.1819(5)	106.317(9)	405.12(6)
5.32(1)	9.4444(7)	8.6152(5)	5.1787(6)	106.290(9)	404.45(7)
5.86(1)	9.4354(7)	8.6024(7)	5.1727(5)	106.243(9)	403.10(6)
6.34(1)	9.4241(9)	8.5935(8)	5.1662(6)	106.12(1)	401.75(7)
6.65(1)	9.420(1)	8.585(1)	5.1637(6)	106.20(1)	401.02(7)
6.99(2)	9.414(1)	8.578(1)	5.1596(6)	106.17(1)	400.15(7)

Table 4.

increasing temperature						*decreasing temperature*					
T (K)	*a* (Å)	*b* (Å)	*c* (Å)	*β* (Å)	*V* (Å^3)	*T* (K)	*a* (Å)	*b* (Å)	*c* (Å)	*β* (Å)	*V* (Å^3)
303	9.5611(7)	8.7387(5)	5.2485(3)	106.855(6)	419.68(5)	1023	9.6228(8)	8.8320(4)	5.2750(3)	106.949(5)	428.84(5)
323	9.5632(5)	8.7410(4)	5.2487(3)	106.856(5)	419.90(4)	973	9.6195(6)	8.8239(4)	5.2727(3)	106.939(4)	428.14(4)
373	9.5662(5)	8.7463(4)	5.2504(2)	106.867(4)	420.40(3)	923	9.6127(8)	8.8175(5)	5.2711(3)	106.941(5)	427.39(5)
423	9.5701(5)	8.7521(4)	5.2523(3)	106.874(4)	420.98(4)	873	9.6077(7)	8.8104(4)	5.2690(3)	106.934(5)	426.67(5)
473	9.5741(5)	8.7581(4)	5.2536(3)	106.877(4)	421.55(4)	823	9.6028(8)	8.8042(4)	5.2666(3)	106.929(5)	425.97(5)
523	9.5783(5)	8.7648(4)	5.2553(3)	106.882(4)	422.18(4)	773	9.5997(6)	8.7964(5)	5.2642(3)	106.906(5)	425.31(4)
573	9.5826(5)	8.7706(4)	5.2574(3)	106.890(4)	422.80(4)	723	9.5948(6)	8.7903(4)	5.2625(3)	106.907(5)	424.66(4)
623	9.5861(6)	8.7773(5)	5.2592(3)	106.895(5)	423.41(4)	673	9.5903(9)	8.7826(6)	5.2607(5)	106.890(8)	423.98(7)
673	9.5916(4)	8.7839(3)	5.2608(2)	106.899(3)	424.09(3)	623	9.5861(6)	8.7769(4)	5.2589(3)	106.894(5)	423.37(4)
723	9.5957(6)	8.7906(4)	5.2627(3)	106.905(5)	424.74(4)	573	9.5820(5)	8.7708(4)	5.2569(2)	106.890(4)	422.74(3)
773	9.6037(8)	8.8041(5)	5.2666(3)	106.918(6)	426.03(5)	523	9.5778(5)	8.7642(4)	5.2550(3)	106.876(4)	422.12(4)
823	9.6039(8)	8.8039(5)	5.2675(3)	106.928(5)	426.08(5)	473	9.5739(4)	8.7585(3)	5.2533(2)	106.876(3)	421.53(3)
873	9.6087(7)	8.8105(4)	5.2692(3)	106.932(5)	426.74(4)	423	9.5698(6)	8.752(4)	5.2514(3)	106.860(5)	420.92(4)
923	9.6132(8)	8.8179(4)	5.2709(3)	106.937(5)	427.42(5)	373	9.5654(7)	8.7443(5)	5.2504(3)	106.861(5)	420.28(5)
973	9.6186(9)	8.8239(5)	5.2728(4)	106.939(5)	428.11(5)	323	9.5623(6)	8.7397(4)	5.2478(4)	106.857(6)	419.72(5)
1023	9.6231(9)	8.8313(5)	5.2749(4)	106.946(7)	428.82(6)	303	9.5616(7)	8.7376(5)	5.2475(4)	106.840(6)	419.60(5)
1073	9.6284(7)	8.8389(4)	5.2774(3)	106.963(5)	429.59(5)						

Table 5.

	N3 [1]	Jd [2]	Di [3]
a_0	9.5740(9)		
Ka_0	111(3)		
K'	8(1)		
b_0	8.7485(5)		
Kb_0	106(2)		
K'	3.9(6)		
c_0	5.2520(7)		
Kc_0	113(3)		
K'	5(1)		
V_0	421.04(7)	402.26(2)	438.80(3)
K_{TO}	119(2)	134.0(7)	106(1)
K'	5.7(6)	4.4(1)	6.1(5)

References [1] sample N3, this work; [2] Nestola et al. (2006); [3] Gavrilenko et al. (2010)

Table 6.

chemical composition	T_r(K)	$V_{Tr\ (exp)}$	Gottschalk (1997)			Holland-Powell (1998)				ref. *
			α_{rT}	V_{Tr}	χ^2	α_{rT}	a_0	V_{Tr}	χ^2	
$Di_{44}Jd_{56}$	303	419.68(5)	3.03(3)	419.46(5)	0.228	2.157	5.07(2)	419.77(2)	0.047	[1]
Jd_{100}	298	402.33(9)	2.54(6)	402.2(1)	0.166	1.826	4.34(4)	402.40(6)	0.054	[2]
Di_{100}	297	439.1(2)	3.37(9)	438.(2)	0.604	2.372	5.65(9)	439.2(1)	0.244	[3]

chemical composition	T_r(K)	$V_{Tr\ (exp)}$	Fei (1995)					Berman (1988)				ref. *
			α_{rT}	a_0	a_1	V_{Tr}	χ^2	$\alpha_{rT} = a_1$	a_2	V_{Tr}	χ^2	
$Di_{44}Jd_{56}$	303	419.68(5)	2.64	2.33(4)	1.02(6)	419.64(2)	0.013	2.64(2)	5.6(3)	419.64(2)	0.012	[1]
Jd_{100}	298	402.33(9)	2.12	1.7(3)	1.4(4)	402.37(8)	0.051	2.1(1)	7.3(2.1)	402.37(8)	0.051	[2]
Di_{100}	297	439.1(2)	2.75	2.3(4)	1.5(6)	439.1(2)	0.289	2.8(2)	8.3(3.0)	439.1(2)	0.287	[3]

Volume thermal expansion coefficients α, a_0 is to be multiplied by $10^{-5}K^{-1}$, a_1 by $10^{-8}K^{-2}$, and a_2 by $10^{-9}K^{-2}$ (*****) data re-calculated using original *T-V* data reported by the authors. (*) references [1] sample N2, this work; [2] Tribaudino et al. (2008); [3] Finger et al. (1976)

Figure

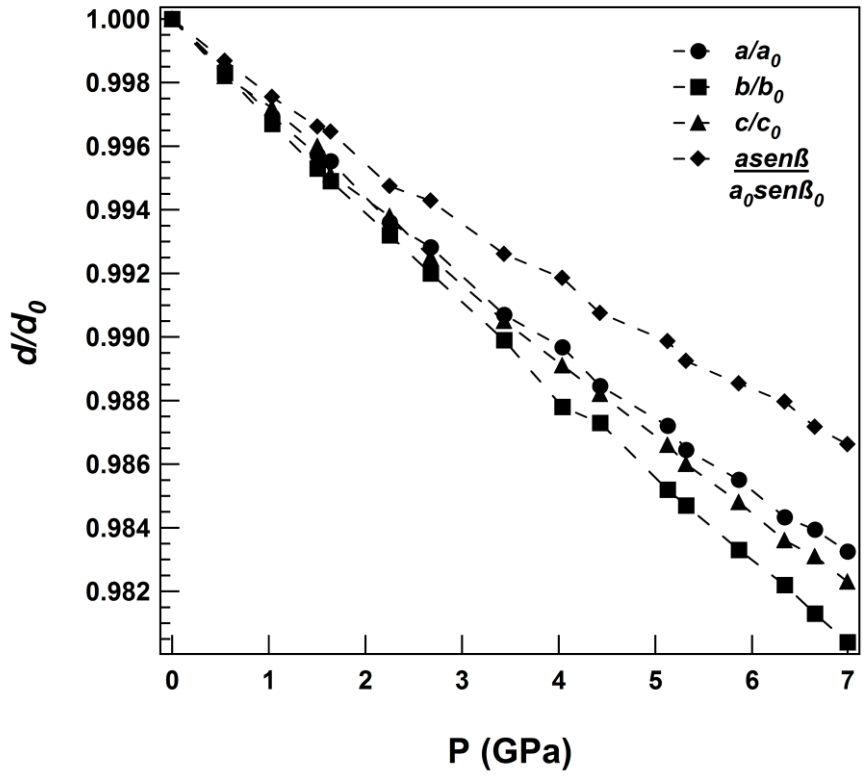

Figure 1.

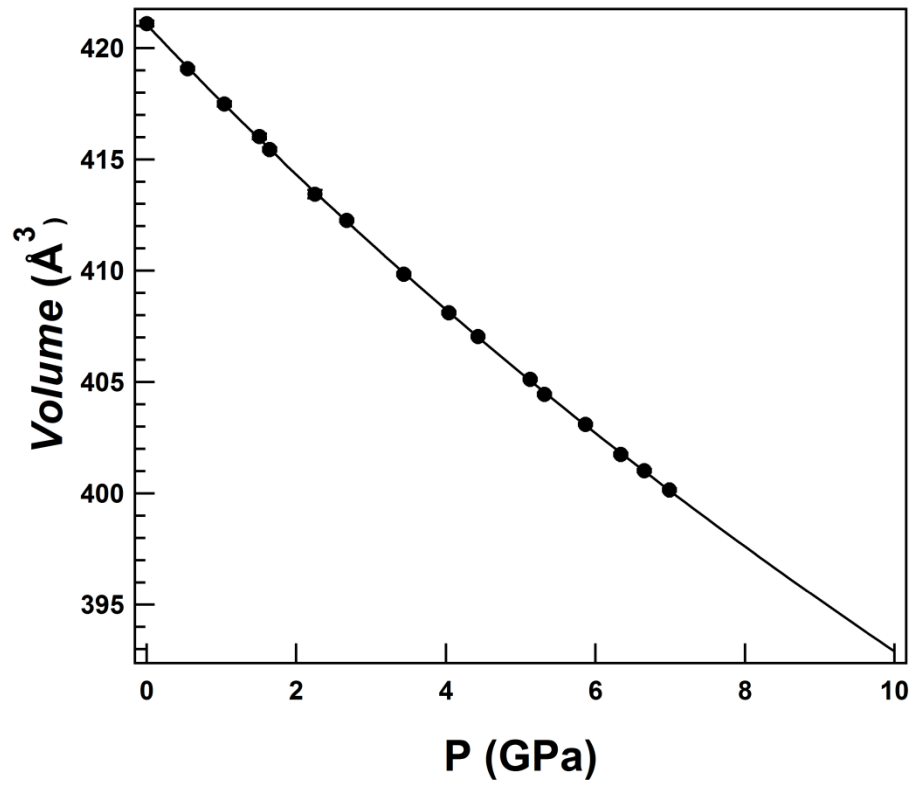

Figure 2.

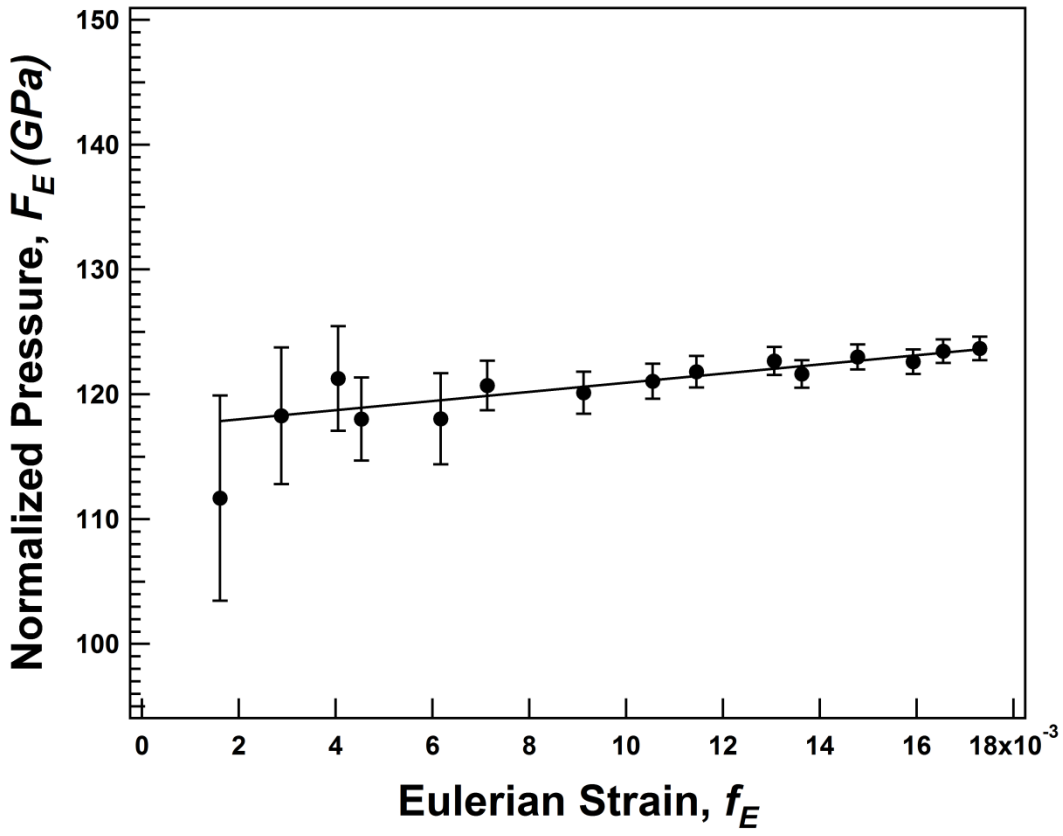

Figure 3.

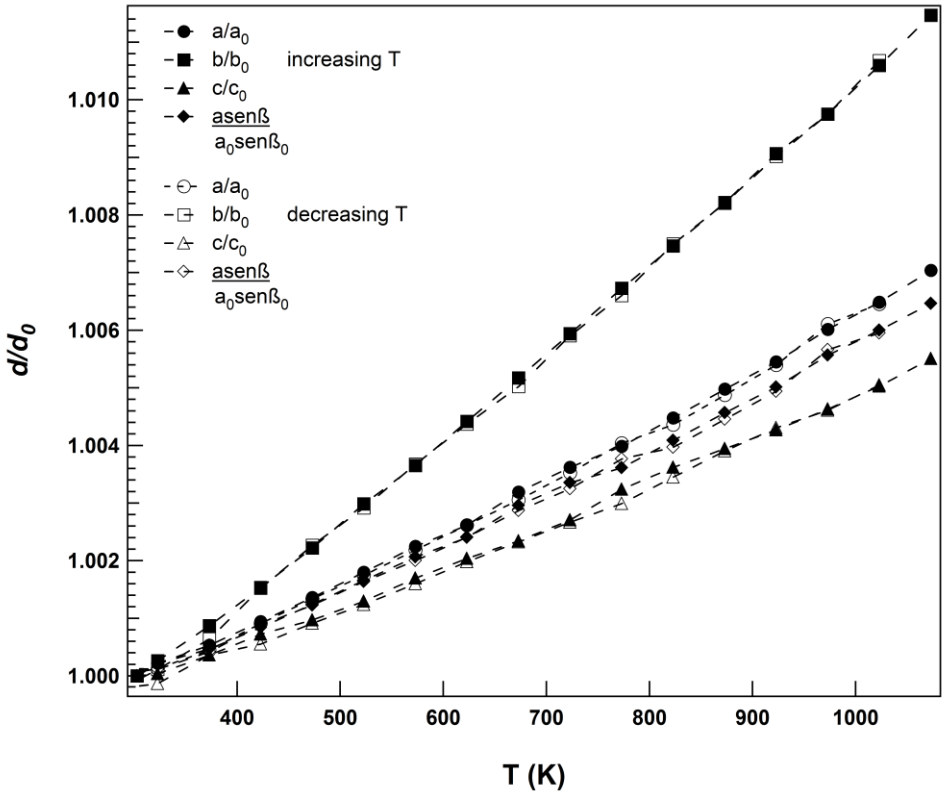

Figure 4.

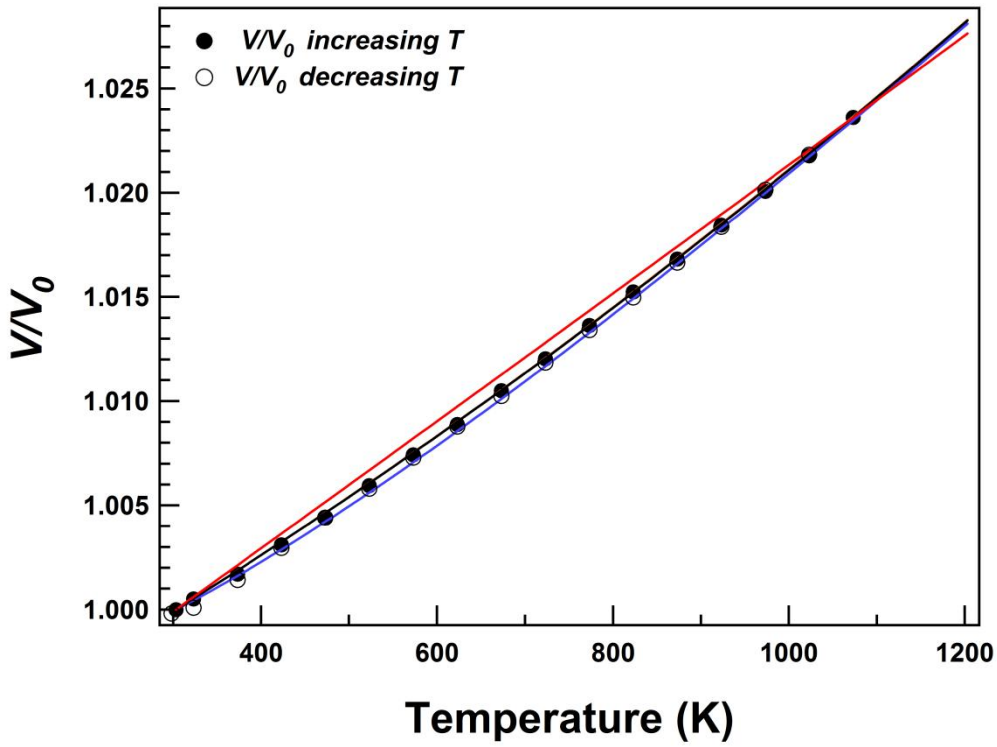

Figure 5.

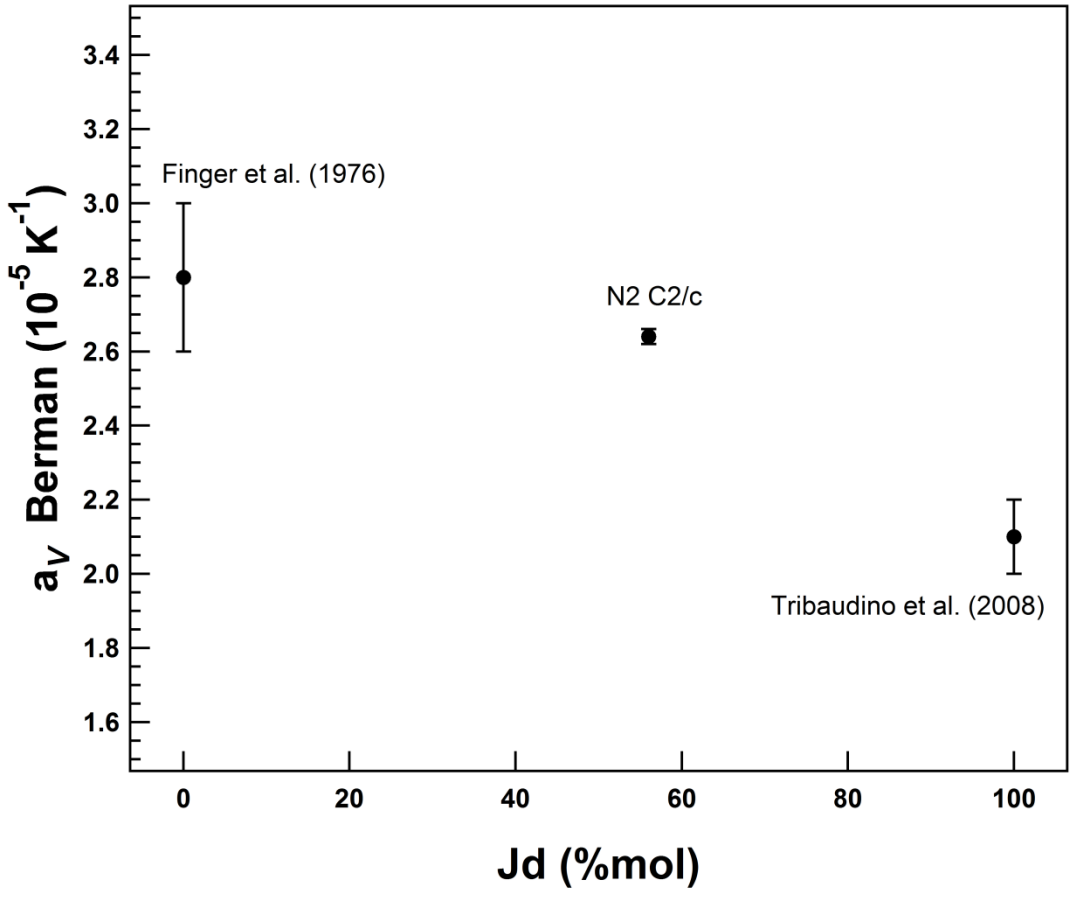

Figure 6.

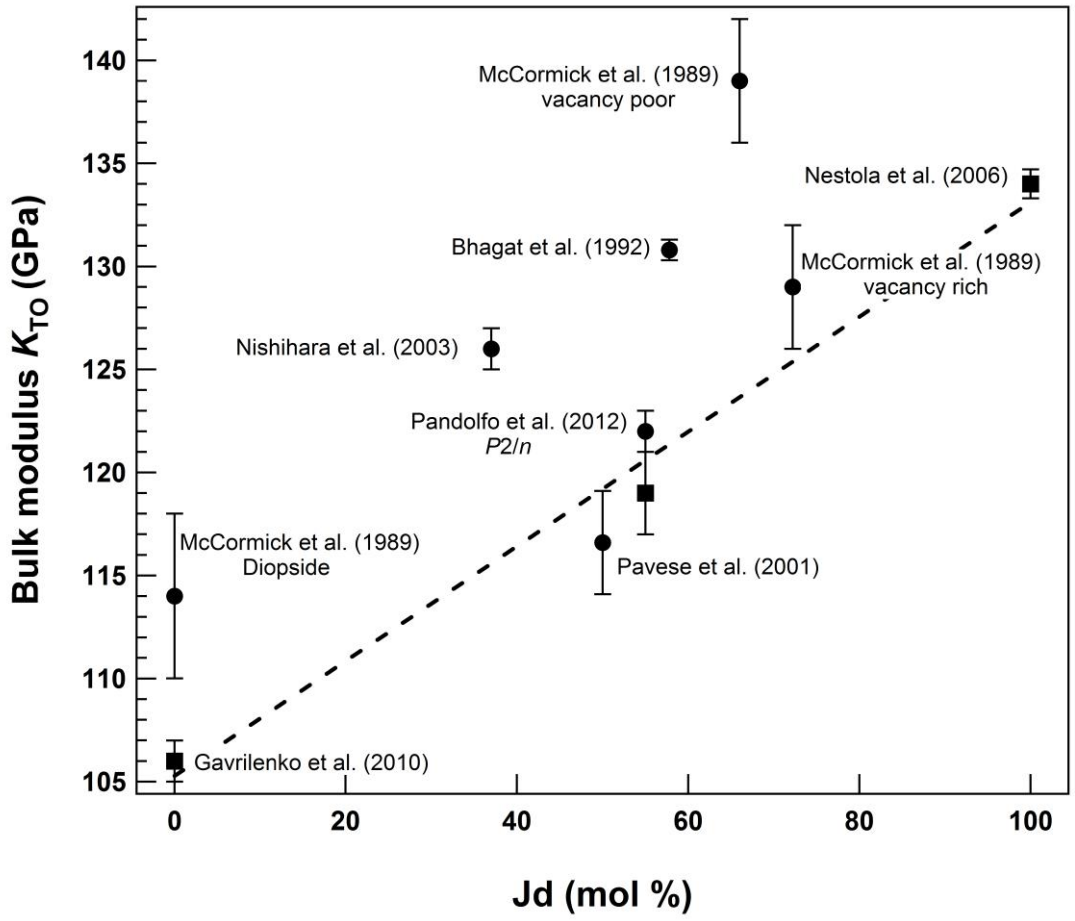
Bulk modulus K_{TO} (GPa)
Jd (mol %)
140
135
130
125
120
115
110
105
0
20
40
60
80
100
McCormick et al. (1989)
vacancy poor
Nestola et al. (2006)
Bhagat et al. (1992)
McCormick et al. (1989)
vacancy rich
Nishihara et al. (2003)
Pandolfo et al. (2012)
P2/n
McCormick et al. (1989)
Diopside
Pavese et al. (2001)
Gavrilenko et al. (2010)

Figure 7.